**Supporting Information**

# Step-scheme photocatalyst of $CsPbBr_3$/BiOBr with oxygen vacancy for efficient $CO_2$ photoreduction

Wanjun Sun,[*a,c] Jifei Liu,[a] Feitian ran,[a] Na Li,[*a] Zengpeng Li,[c] Yuanyuan Li,[*b] Kai Wang[*a]

[a] School of New Energy and Power Engineering, Lanzhou Jiaotong University, Lanzhou, Gansu, 730070, China

[b] Department of Biological and Chemical Engineering, Chongqing University of Education, Chongqing 400067, China.

[c] Key Laboratory of Solar Power System Engineering, Jiuquan Vocational and Technical College, Jiuquan, 735000, China

Corresponding author.

E-mail addresses: wanjunsun@mail.lzjtu.cn, lin19@lzu.edu.cn, liyy@cque.edu.cn, wangk@mail.lzjtu.cn

## Materials

Bismuth nitrate pentahydrate ($Bi(NO_3)_3 \cdot 5H_2O$) and ethylene glycol ($(CH_2OH)_2$) were purchased from Aladdin. Potassium bromide (KBr), polyvinylpyrrolidone (PVP, M.W. 30K), CsBr, $PbBr_2$, oleylamine, oleic acid and N, N-Dimethylformamide (DMF) were obtained from Energy Chemical Reagent. All chemicals were of analytical grade purity.

## Characterization

The crystalline phase of the samples was characterized by X-ray diffraction (XRD, Bruker D8 X, Germany) which was equipped with Cu-Kα. The morphology and microstructure of the as-prepared samples were detected by scanning electron microscopy (SEM, Zeiss Gemini 500) and transmission electron microscope (TEM) (FEI Tecnai F30). Elemental analysis of the sample was determined on TJA ICP-atomic emission spectrometer (IRIS Advantage ER/S). High resolution X-ray photoelectron spectroscopy (XPS) data were measured using Axis Supra® and the binding energy of all the elements were corrected by the C 1s peak (284.8 eV). UV-vis diffuse reflectance spectra (UV-vis DRS) were recorded on a Shimadzu UV-2600 spectrophotometer equipped with integrating spheres. The electron paramagnetic resonance (EPR) spectra were obtained on a Bruker EMXPlus Spectrometer.

**Photoelectrochemical measurements**

The working electrode was fluorine doped tin oxide (FTO) glass coated with sample aqueous solution. First, 5 mg of catalyst was dispersed in 1 mL of tetrabutylammonium hexafluorophosphate ($TBAPF_6$)/ethyl acetate solution by sonication for 1 h to obtain a slurry. Then, 100 μL slurry were dropped onto a 1 cm × 2 cm FTO glass electrode. The FTO glass was dried at 60 °C for 30 min. Afterwards, 10 μL 0.5% Nafion was deposited on the working electrode to enhance improve the adhesion. All photoelectrochemical measurements were performed on a CHI 660D workstation (CH Instruments Co.) under irradiation of a 300 W Xe lamp (AM1.5G, and 100 mW $cm^{-2}$) at open circuit voltage. A standard three-electrode cell was employed with a Pt wire as the counter electrode and an Ag/AgCl electrode as the reference electrode. 0.05 M tetrabutylammonium hexafluorophosphate ($TBAPF_6$)/ethyl acetate solution was filled in the quartz cell as the electrolyte. I-t curves were carried out at a bias potential of 0.1 V vs. Ag/AgCl. Electrochemical impedance spectroscopy (EIS) was conducted under a frequency range of 0.01-$10^5$ Hz.

**Calculation of the lifetime of the photogenerated carrier**

The decay curves obtained from TRPL can be well fitted by the following three-exponential equation:

$$I_{(t)} = I_{(0)} + A_1\exp(-t/\tau_1) + A2\exp(-t/\tau_2) + A_3\exp(-t/\tau_3)$$

where the $I_0$ represents the baseline correction value, $A_1$, $A_2$, and $A_3$ are the pre-exponential factors, and $\tau_1$, $\tau_2$ represent the lifetime of the radiant energy transfer process (ns), while $\tau_3$ represents the lifetime of the non-radiative energy transfer process (ns). The average lifetime ($\tau_{ave}$) can be calculated according to the following equation:

$$\tau_{ave} = (A_1\tau^2_1 + A_2\tau^2_2 + A_3\tau^2_3)/(A_1\tau_1 + A_2\tau_2 + A_3\tau_3)$$

## Computational detail

DFT calculations were conducted through the Vienna ab initio Simulation Package (VASP) with the projector augment wave method [1, 2]. Generalized gradient approximation of the Perdew-Burke-Ernzerhof (PBE) functional was used as the exchange-correlation functional [3]. The Brillouin zone was sampled with 2 × 2 × 1 K points for surface calculation [4]. The cutoff energy was set as 500 eV, and structure relaxation was performed until the convergence criteria of energy and force reached $1 \times 10^{-5}$ eV and 0.02 eV $Å^{-1}$, respectively. A vacuum layer of 15 Å was constructed to eliminate interactions between periodic structures of surface models. The van der Waals (vdW) interaction was amended by the zero damping DFT-D3 method of Grimme [5].

The adsorption energy ($\Delta E_{ads}$) of adsorbate adsorption on surface is defined as: $\Delta E_{ads} = E(*adsorbate) - E(*) - E(adsorbate)$

where E(*adsorbate) and E(*) are the total energy of surface systems with and without adsorbate, respectively, E(adsorbate) is the energy of an isolated adsorbate. According to this definition, negative adsorption energy suggests that the adsorption process is exothermic and the adsorption system is thermodynamically stable. Contrarily, a positive value corresponds to an endothermic and unstable adsorption.

### *In-situ* DRIFT measurements

In-situ DRIFT experiment was performed on a Bruker Vertex 70 Fourier Transform Infrared Spectrometer. The prepared sample was placed in a reaction cell and pretreated with argon gas at 150 °C for 30 min to remove impurities. Then the reaction cell was cooled to room temperature, the background spectrum was taken, and then the mixture of $CO_2$ and water vapor was passed into the reaction cell for adsorption. After 20 min, 300 W Xe lamp with an optical cutoff filter ($\lambda > 420$ nm) were applied to irradiate, and FTIR spectra were collected over time.

## Femtosecond transient absorption (fs-TA) measurements

For fs-TA spectroscopy, the laser source was a Coherent Legend Elite regenerative amplifier (<110 fs, 1 KHz, 800 nm) that was seeded by a Coherent Chameleon oscillator (75 fs, 80 MHz). The white probe pulses in 330-600 nm range were generated on a CaF2 crystal excited by partial of the 800-nm laser beam from the amplifier. The 300 nm and 440 nm pump pulse were generated from a Light Conversion OPerA-Solo optical parametric amplifier (285-2600 nm). The polarization between 300-nm pump and probe was set at the magic angle of 54.7° or the pump was directly depolarized (for pump>350 nm) to remove the artifacts of orientational relaxation. The data were fitted using Surface Xplore software (Ultrafast Systems, LLC). The samples were stored in a quartz cuvette for TA measurement. All of the measurements were performed at room temperature unless otherwise specified.

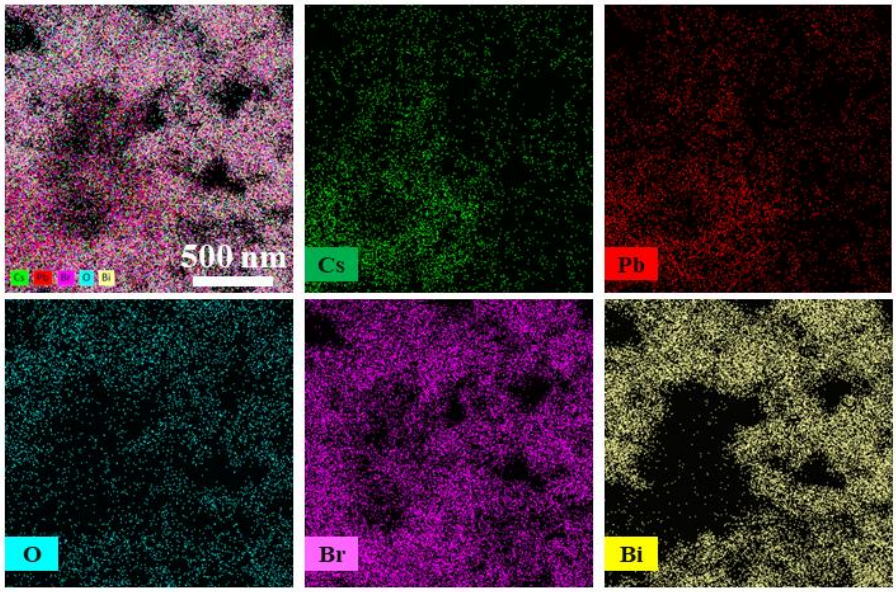


**Fig. S1**. EDS mappings of $CsPbBr_3$/BiOBr-Ov.

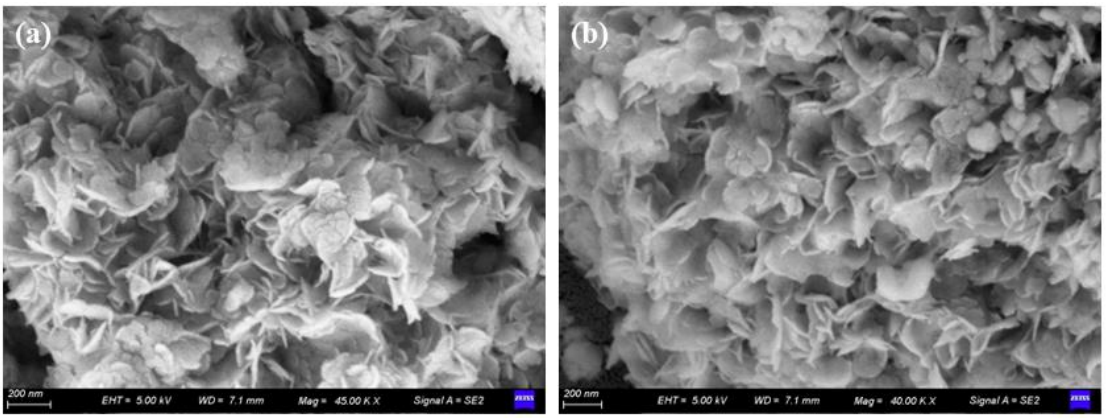


**Fig. S2**. The SEM images of (a) BiOBr-Ov and (b) $CsPbBr_3$/BiOBr-Ov-2, respectively.

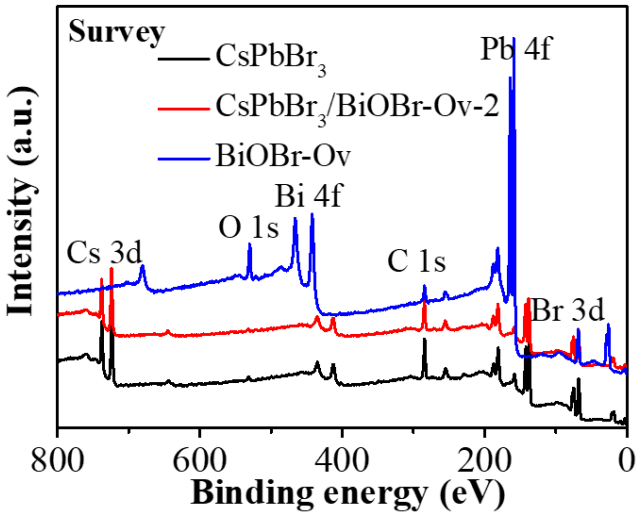


**Fig. S3**. XPS spectra of survey scan of $CsPbBr_3$, BiOBr-Ov and $CsPbBr_3$/BiOBr-Ov-2, respectively.

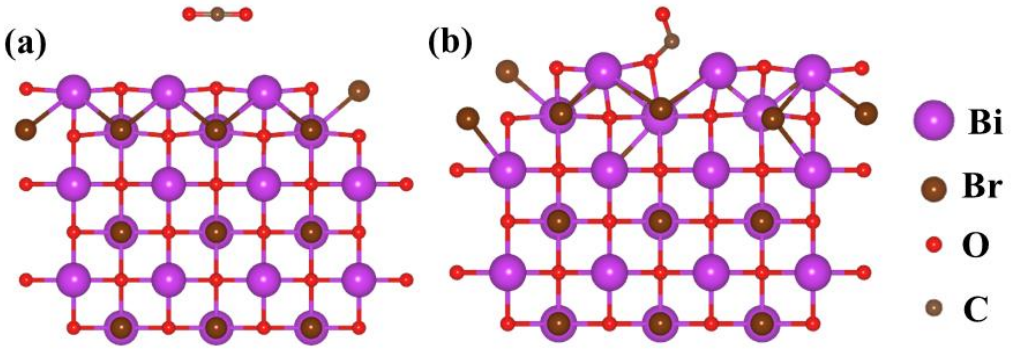


**Fig. S4**. Top view the optimized (a) BiOBr, (b) BiOBr-Ov adsorbed with $CO_2$.

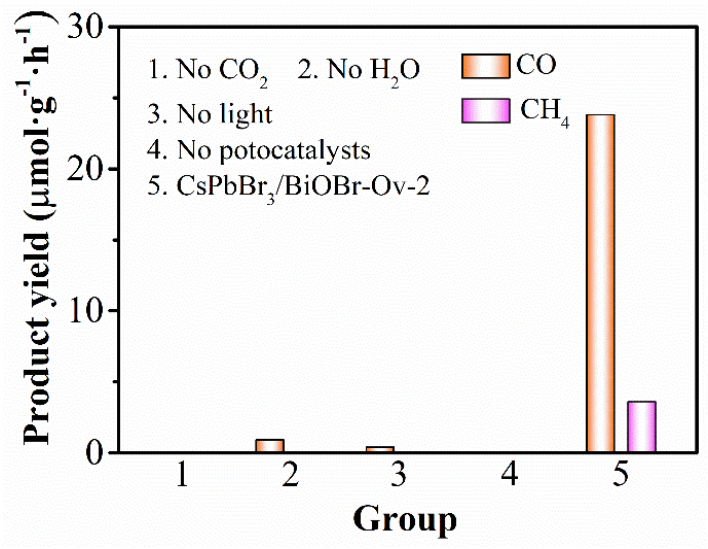


**Fig. S5**. $CO_2$ photoreduction performance under different conditions.

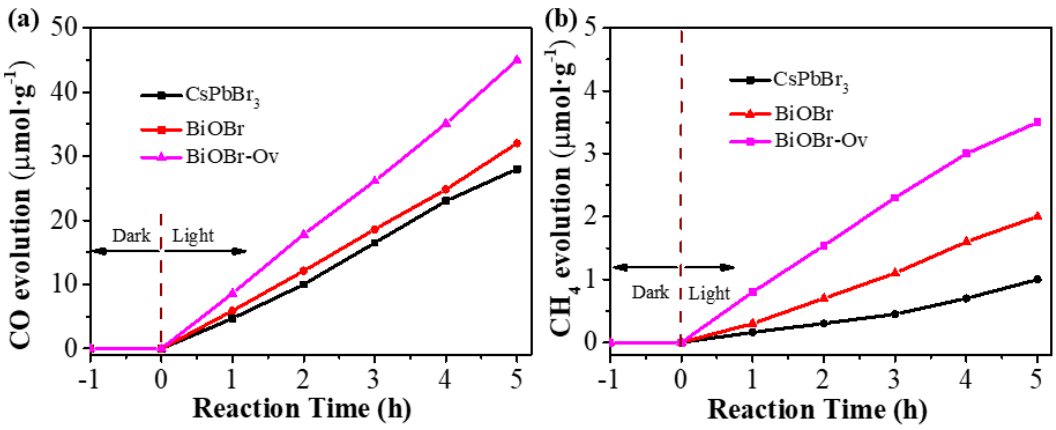


**Fig. S6**. Time-dependent of photocatalytic (a) CO and (b) $CH_4$ production over $CsPbBr_3$, BiOBr, and BiOBr-Ov, respectively.

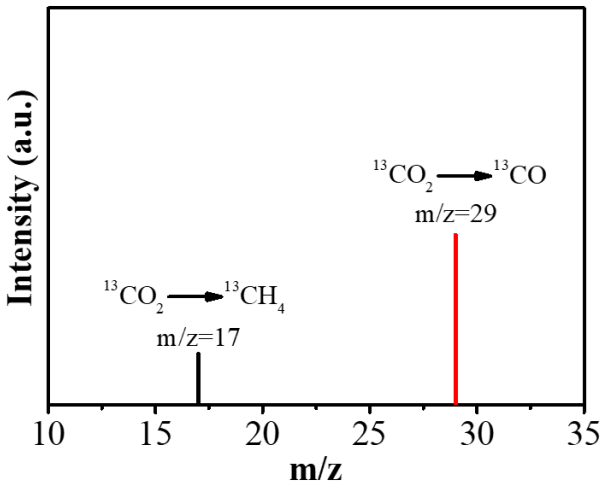


**Fig. S7**. GC-MS spectra analysis of $^{13}CO_2$ to $^{13}CH_4$ and $^{13}CO$ using $CsPbBr_3$/BiOBr-Ov-2 as a photocatalyst.

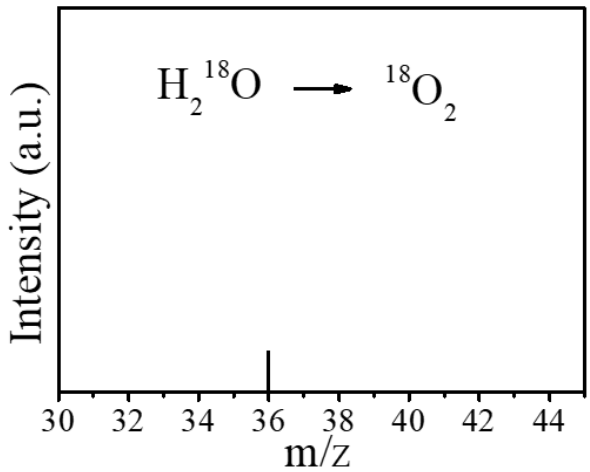


**Fig. S8**. Gas chromatogram and mass spectra (GC-MS) analysis for solar-driven oxidation of $H_2{}^{18}O$ to $^{18}O_2$ (m/z = 36) using $CsPbBr_3$/BiOBr-Ov-2 as a photocatalyst.

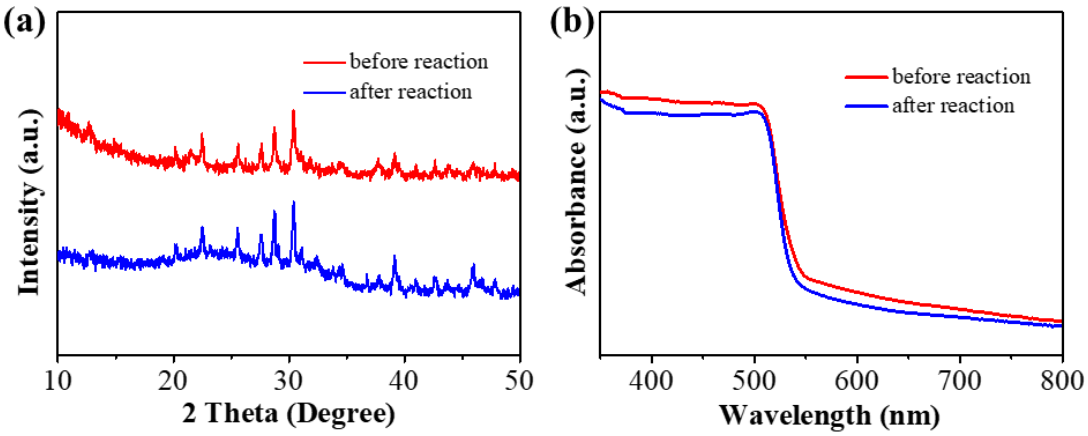


**Fig. S9**. (a) XRD patterns and (b) UV-vis DRS spectra of $CsPbBr_3$/BiOBr-Ov-2 before and after cycling experiment.

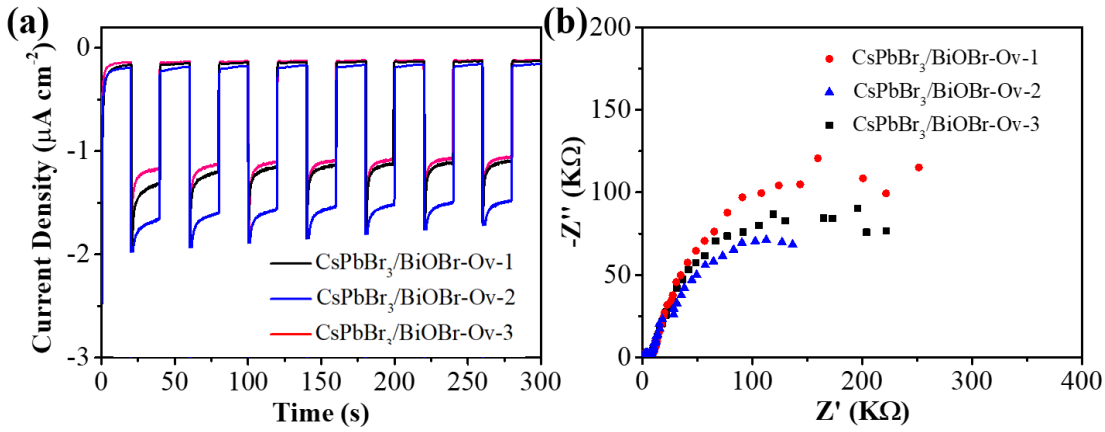


**Fig. S10**. (a) Transient photocurrent measurement and (b) EIS plot for as-prepared $CsPbBr_3$/BiOBr-Ov sample.

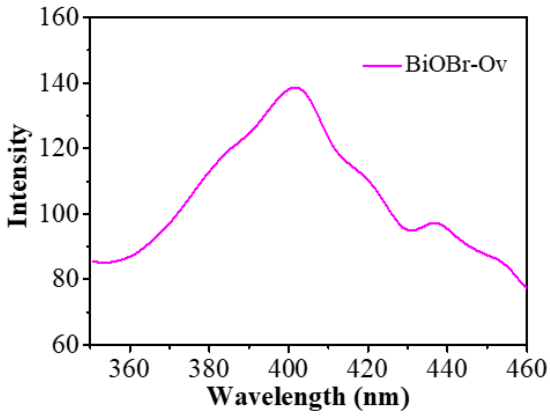


**Fig. S11**. Steady-state PL spectra of BiOBr-Ov.

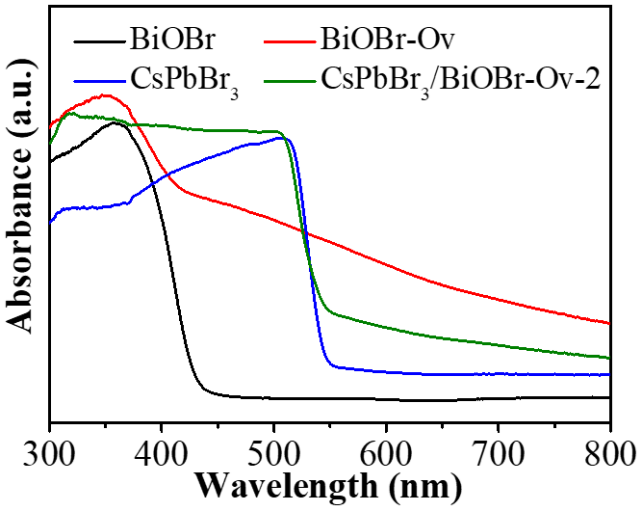


**Fig. S12**. UV–visible diffuse reflectance spectra of BiOBr, BiOBr-Ov, $CsPbBr_3$ and $CsPbBr_3$/BiOBr-Ov-2, respectively.

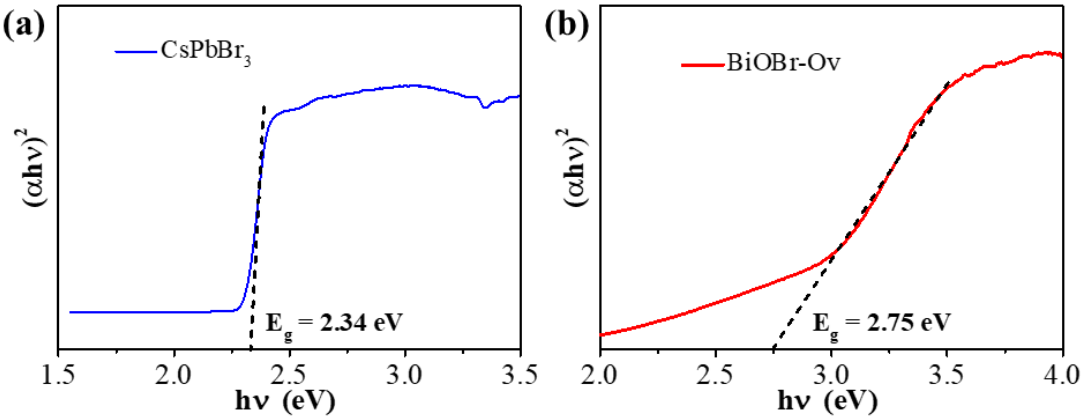


**Fig. S13**. Tauc-plot of (a) $CsPbBr_3$ and (b) BiOBr-Ov, respectively.

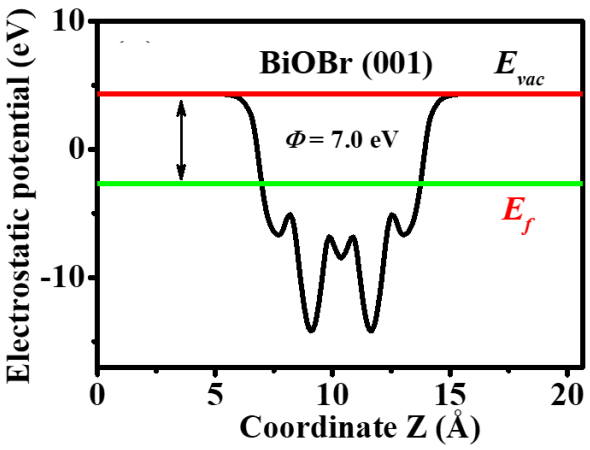


**Fig. S14**. The work functions of BiOBr.

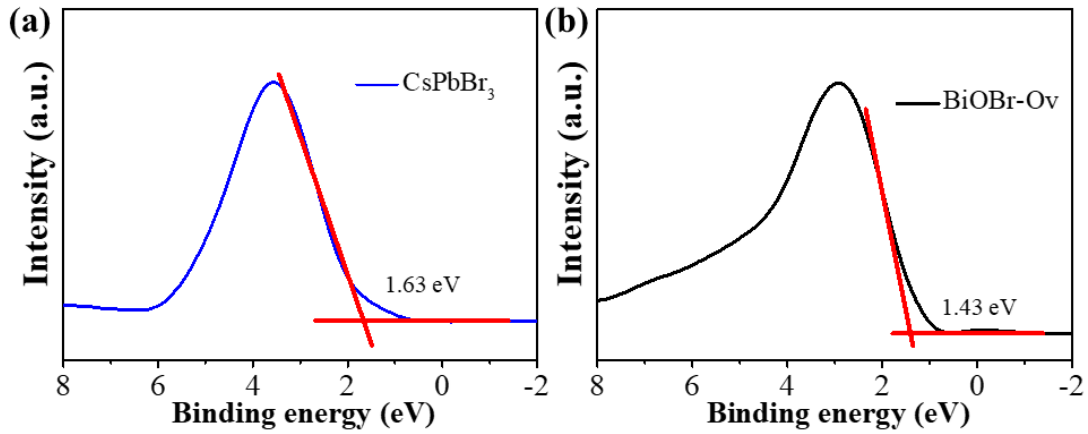


**Fig. S15**. XPS valence band spectra of (a) $CsPbBr_3$ and (b) BiOBr-Ov, respectively.

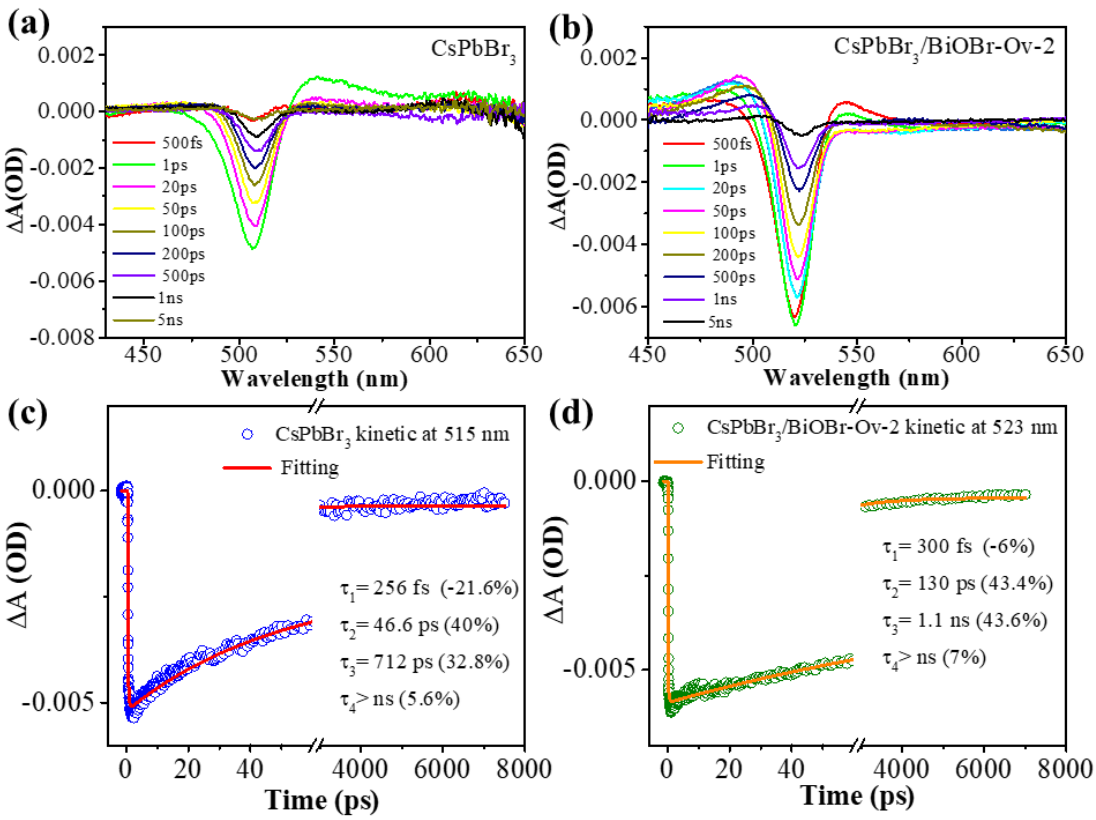


**Fig. S16**. Representative spectra at different delay time for the $CsPbBr_3$ QDs (a), $CsPbBr_3$/BiOBr-Ov-2 (b) in the range of 500 fs-5 ns. The kinetic traces of $CsPbBr_3$ QDs for 515 nm (c) and $CsPbBr_3$/BiOBr-Ov-2 for 523 nm (d) excited at 300 nm.

**Table S1**. The calculated $CO_2$ adsorption energy values on surfaces of BiOBr and BiOBr-Ov.

| Sample | E(*) (eV) | E($CO_2$) (eV) | E(*$CO_2$) (eV) | $\Delta E_{ads}$(eV) |
|---|---|---|---|---|
| BiOBr | -247.767 | -22.9548 | -270.924 | -0.20205 |
| BiOBr-Ov | -239.621 | -22.9538 | -262.947 | -0.37069 |

**Table S2**. Summary of the $CsPbBr_3$ and BiOBr-based photocatalysts $CO_2$ reduction.

| photocatalyst | Light source | Reduction medium | Products (μmol $g^{-1}$ $h^{-1}$) CO | $CH_4$ | $R_{electron}$ (μmol $g^{-1}$ $h^{-1}$) | Reference |
|---|---|---|---|---|---|---|
| $SnS_2/CsPbBr_3$ | Xe lamp (λ=300–800 nm) | $H_2O$ | 1.98 | -- | 3.96 | [6] |
| CPB@ZIF-8 | | EA/$H_2O$ | 1.52 | 5.43 | 15.5 | [7] |
| $TiO_2/CsPbBr_3$ | 300 W Xe lamp (UV-vis light) | ACN/$H_2O$ | 9.02 | | 18.99 | [8] |
| $CsPbBr_3$@ZIF-67 | AM 1.5G, 150 mW $cm^{-2}$ | gas solid phase, water | 0.77 | 3.51 | 29.63 | [9] |
| $CsPbBr_3$/GO | 100 W Xe lamp, (AM 1.5G filter) | Liquid-solid, ethyl acete | 4.89 | 2.47 | 29.8 | [10] |
| $CsPbBr_3$/NiFe-LDH | | | 13.14 | | 39.58 | [11] |
| $CsPbBr_3/Au/TiO_2$ | A 300 W Xe lamp | $H_2O$ | 17.27 | 1.22 | 44.3 | [12] |
| $CsPbBr_3/In_2O_3$ | 300 W Xe lamp (AM 1.5G filter) | EA/$H_2O$ | 12.50 | 3.87 | 55.96 | [13] |
| BiOBr/$Zn(OH)_2$ | 300 W Xe lamp (λ>420 nm) | Liquid-solid, water | 5.4 | -- | 10.8 | [14] |
| BiOCl/BiOBr | 380 nm | Liquid-solid, water | 7.4 | -- | 14.8 | [15] |
| BiOBr/$NH_2$-UiO-66 | 300 W Xe lamp | Liquid-solid, water | 9.19 | -- | 18.38 | [16] |
| BiOBr/TCN | 300 W Xe lamp (λ>400 nm) | Liquid-solid, water | 10.89 | -- | 21.78 | [17] |
| Co-BiOBr | 300 W Xe lamp (λ>420 nm) | Liquid-solid, water | 11.71 | -- | 23.42 | [18] |
| AgBr/BiOBr | 300 W Xe lamp (λ>420 nm) | Liquid-solid, water | 12.43 | -- | 24.86 | [19] |
| $Bi_{19}S_{27}Br_3$/BiOBr | 300 W Xe lamp | Liquid-solid, water | 19.83 | -- | 39.66 | [20] |
| $CsPbBr_3$/BiOBr-Ov-2 | 300 W Xe lamp (100 mW $cm^{-2}$) | EA/$H_2O$ | 23.8 | 3.6 | 76.4 | **This work** |

## Refences


[1] P.E. Blöchl, Projector augmented-wave method, *Phys. Rev. B*, **1994**, *50*, 17953-17979.

[2] G. Kresse, D. Joubert, From ultrasoft pseudopotentials to the projector augmented-wave method, *Phys. Rev. B*, **1999**, *59*, 1758-1775.

[3] J.P. Perdew, K. Burke, M. Ernzerhof, Generalized Gradient Approximation Made Simple, *Phys. Rev. Lett.*, **1996**, *77*, 3865-3868.

[4] V. Wang, N. Xu, J.-C. Liu, G. Tang, W.-T. Geng, VASPKIT: A user-friendly interface facilitating high-throughput computing and analysis using VASP code, *Computer Physics Communications*, **2021**, *267*, 108033.

[5] S. Grimme, S. Ehrlich, L. Goerigk, Effect of the damping function in dispersion corrected density functional theory, **2011**, *32*, 1456-1465.

[6] R. Zhang, L. Li, Y. Li, D. Wang, Y. Lin, T. Xie, Z-scheme $SnS_2/CsPbBr_3$ Heterojunctions for Photoreduction $CO_2$ Reaction and Related Photoinduced Carrier Behaviors, *Solar RRL*, **2022**, *6*, 2200536.

[7] Y. Xi, X. Zhang, Y. Shen, W. Dong, Z. Fan, K. Wang, S. Zhong, S. Bai, Aspect ratio dependent photocatalytic enhancement of $CsPbBr_3$ in $CO_2$ reduction with two-dimensional metal organic framework as a cocatalyst, *Appl. Catal. B Environ.*, **2021**, *297*, 120411.

[8] F. Xu, K. Meng, B. Cheng, S. Wang, J. Xu, J. Yu, Unique S-scheme heterojunctions in self-assembled $TiO_2/CsPbBr_3$ hybrids for $CO_2$ photoreduction, *Nat. Commun.*, **2020**, *11*, 4613.

[9] Z.-C. Kong, J.-F. Liao, Y.-J. Dong, Y.-F. Xu, H.-Y. Chen, D.-B. Kuang, C.-Y. Su, Core@Shell $CsPbBr_3$@Zeolitic Imidazolate Framework Nanocomposite for Efficient Photocatalytic $CO_2$ Reduction, *ACS Energy Lett.*, **2018**, *3*, 2656-2662.

[10] Y.F. Xu, M.Z. Yang, B.X. Chen, X.D. Wang, H.Y. Chen, D.B. Kuang, C.Y. Su, A $CsPbBr_3$ perovskite quantum dot/graphene oxide composite for photocatalytic $CO_2$ reduction, *J. Am. Chem. Soc.*, **2017**, *139*, 5660-5663.

[11] H. Sun, R. Tang, X. Zhang, S. Zhang, W. Yang, L. Wang, W. Liang, F. Li, R.

Zheng, J. Huang, Interfacial energy band engineered $CsPbBr_3$/NiFe-LDH heterostructure catalysts with tunable visible light driven photocatalytic $CO_2$ reduction capability, *Catal. Sci. Technol.*, **2023**, *13*, 1154-1163.

[12] W. Song, K.C. Chong, G. Qi, Y. Xiao, G. Chen, B. Li, Y. Tang, X. Zhang, Y. Yao, Z. Lin, Z. Zou, B. Liu, Unraveling the Transformation from Type-II to Z-Scheme in Perovskite-Based Heterostructures for Enhanced Photocatalytic $CO_2$ Reduction, *J. Am. Chem. Soc.*, **2024**, *146*, 3303-3314.

[13] J. Ding, X. Deng, J. Fan, Y. Wang, Z. Li, Q. Liang, Embedding $CsPbBr_3$ Quantum Dots into an $In_2O_3$ Nanotube for Selective Photocatalytic $CO_2$ Reduction to Hydrocarbon Fuels, *Inorg. Chem.*, **2023**, *62*, 16493-16502.

[14] W. Qin, Q. Yang, H. Ye, Y. Xie, Z. Shen, Y. Guo, Y. Deng, Y. Ling, J. Yu, G. Luo, N. Raza, W. Raza, J. Zhao, Novel 2D/2D BiOBr/$Zn(OH)_2$ photocatalysts for efficient photoreduction $CO_2$, *Separation and Purification Technology*, **2023**, *306*, 122721.

[15] Y. Wu, M. Xu, Y. Wang, B. Hu, Y. Xie, Y. Ling, BiOCl/BiOBr composites for efficient photocatalytic carbon dioxide reduction, *Applied Catalysis A: General*, **2024**, *677*, 119708.

[16] J. Liu, W. Qin, Y. Wang, Q. Xu, Y. Xie, Y. Chen, Y. Dai, W. Zhang, $NH_2$-UiO-66 modification BiOBr enhancement photoreduction $CO_2$ to CO, *Separation and Purification Technology*, **2024**, *344*, 127289.

[17] W. Tao, Q. Tang, J. Hu, Z. Wang, B. Jiang, Y. Xiao, R. Song, S. Guo, Construction of a hierarchical BiOBr/$C_3N_4$ S-scheme heterojunction for selective photocatalytic $CO_2$ reduction towards CO, *J. Mater. Chem. A*, **2023**, *11*, 24999-25007.

[18] Y. Xie, Y. Wang, Y. Zhou, F. Wang, Y. Xu, S. Rao, J. Zhao, Cation exchange strategy to construct Co-doped BiOBr nanosheets for high-efficient photocatalytic $CO_2$ to CO, *Applied Catalysis A: General*, **2024**, *669*, 119504.

[19] Y. Xie, Y. Zhou, C. Gao, L. Liu, Y. Zhang, Y. Chen, Y. Shao, Construction of AgBr/BiOBr S-scheme heterojunction using ion exchange strategy for high-efficiency reduction of $CO_2$ to CO under visible light, *Separation and Purification Technology*, **2022**, *303*, 122288.

[20] J. Zhao, M. Xue, M. Ji, B. Wang, Y. Wang, Y. Li, Z. Chen, H. Li, J. Xia,

“Electron collector” $Bi_{19}S_{27}Br_3$ nanorod-enclosed BiOBr nanosheet for efficient $CO_2$ photoconversion, *Chin. J. Catal.*, **2022**, *43*, 1324-1330.